Ionics (2021) 27:2553–2560
https://doi.org/10.1007/s11581-021-04017-w

ORIGINAL PAPER

Straightforward synthesis of chemically ordered Pt_3Co/C nanoparticles by a solid phase method for oxygen-reduction reaction

Zhenzhi Cheng[1,2] · Sen Liao[1] · Weiping Zhou[1] · Guangsheng Luo[1] · Haifu Huang[3]

Received: 17 November 2020 / Revised: 24 February 2021 / Accepted: 22 March 2021 / Published online: 30 March 2021

Abstract

We developed a solid phase method to fabricate structurally ordered Pt_3Co/C nanoparticles (NPs) with controllable component proportion as a high efficiency catalyst toward oxygen-reduction reaction. As a result, Pt_3Co/C NPs exhibit high crystallinity with small average size and narrow size distribution. Moreover, the ordered Pt_3Co/C NPs own enhanced ORR catalytic performance in acid. During the preparation process, the NaCl-matrix acts synergistically with carbon black as nanoreactors for Pt alloying with Co, avoiding serious sintering resulted by annealing at high temperature. Furthermore, other Pt-based NPs supported on carbon can also be prepared by this methodology.

Keywords Pt_3Co/C nanoparticles · Chemical ordered phase · Oxygen-reduction reaction · High-performance catalyst · Solid phase method

Introduction

Proton-exchange membrane fuel cell (PEMFC) has attracted a great deal of attention in energy conversion devices for its zero emission, high energy density, and energy conversion efficiency [1–3]. And the noble metal Pt represents the most widely explored catalyst for its enhanced activity and durability in ORR [4–6]. But the scarcity and high price of precious metals severely hindered the process of commercialization [7]. The problems existing in Pt-based electrocatalysts are needed to be solved urgently. In view of this, various means have been explored, mainly including reducing the loadings of precious metals by decreasing the catalyst particle size, constructing a core-shell or nanowire structure [8–10], enhancing activity and durability by incorporating 3d-transition metals into the Pt crystal lattice [11, 12], or exposing highly active facets on the surface [13]. Previous studies proved that enhanced activity and durability result from modifying Pt electronic structure by incorporation of 3d-transition metals, which lower the d-band center position and suppresses the adsorption of spectator oxygenated species like OH^- simultaneously [14, 15]. It is worth noting that structurally ordered intermetallic Pt-M (Co, Fe, and Ni) electrocatalysts perform the better activity and durability compared with disordered structure [16, 17]. However, the Pt-M alloy NPs prepared by the general strategy often exhibit a disordered phase. To obtain ordered phase, the catalyst should be annealed at high temperature, inevitably resulting in the sintering of NPs. To solve these difficulties, researchers have put forward several approaches. Such as coating the alloy particles with magnesium oxide or silicon dioxide [18, 19] or monodispersing the FePt NPs in the NaCl-matrix by a milling method [20, 21]. Nevertheless, all the pathways mentioned above should synthesize the alloy NPs by a solvothermal method firstly. This process is complex and high technique required and results in consumption of large amount of organic reagents and limited yield. Impregnation is a simple and successful method that can conveniently realize chemically ordered Pt-M NPs with enhanced activity and durability [17, 22]. However, it was accompanied by a long dipping time or a low loading of metal species resulted by the small driving force of mass adsorption on support [23, 24]. And the different adsorption capacities to the support between the ions lead to a difficulty in obtaining rational designed product.

✉ Zhenzhi Cheng
chengzz@ncu.edu.cn

[1] School of Materials Science and Engineering, Nanchang University, Nanchang 330031, People's Republic of China

[2] Nanjing National Laboratory of Solid State Microstructures, Nanjing University, Nanjing 210093, People's Republic of China

[3] Guangxi Novel Battery Materials Research Center of Engineering Technology, School of Physical Science and Technology, Guangxi University, Nanning 530004, People's Republic of China

In our previous work, a new method named salt-assisted spray paint drying method (SPD method) was proposed to achieve facile synthesis of chemically ordered Pt_3Co NPs [25]. However, it also exists in the problem that the prepared NPs are hard to transfer onto the carbon support or achieve a strong combination. To overcome this, we directly dispersed carbon black in the precursor solution and successfully realized straightforward synthesis of ordered Pt_3Co NPs monodispersed on carbon with a mean size of 5.1 nm. In the synthesis, the carbon black monodispersed in micro precursor droplets plays an important role in accelerating drying of droplets for its good thermal conductivity. Furthermore, NaCl-matrixes combining with carbon black serve as nanoreactors for Pt alloying with Co and effectively hamper sintering of Pt_3Co nanopartilces in the high temperature treatment process. As a consequence, the ordered Pt_3Co/C-700 catalyst owns the highest mass activity, corresponding to 2.51-fold enhancements relative to Pt/C for ORR with a mean size of 5.1 nm, while the Pt_3Co/C-500 shows a 1.81 times enhancement. The Pt_3Co/C-700 catalyst possesses an outstanding durability performance, determined to be as low as 15 mV negative shift after 10000 CV cycles in half-wave potential ($E_{1/2}$). However, the Pt_3Co/C-500 catalyst shows approximately 40 mV.

Experiments

Materials

NaCl (99.9%), $Co(NO_3)_2{\cdot}6H_2O$ (99.9%), and polyvinylpyrrolidone (PVP, K16-18, MW~8000) were all purchased from Aladdin Reagent company. In addition, $HClO_4$ (70%, GR) and $H_2PtCl_6{\cdot}6H_2O$ came from Sinopharm Chemical Reagent company. Pt/C (20% Pt) was bought from Johnson Matthey. Vulcan XC-72R carbon black was purchased from Cabot Corporation.

Preparation of Pt_3Co/C NPs

Pt_3Co/C NPs were successfully prepared via a solid phase method. Typically, $Co(NO_3)_2{\cdot}6H_2O$ (187.3 mg), $H_2PtCl_6{\cdot}6H_2O$ (1 g), and NaCl (5.93 g) were dissolved in 50 mL deionized water at ambient condition by stirring. Then, 1.66 g Vulcan XC-72R and 1.66 g PVP were added into the solution. After stirring for 20 min, the precursor solution was sprayed onto a heated quartz plate (270°C). A uniformly mixed salt precursor was formed at the surface of quartz plate for the water evaporated off immediately. Afterward, the mixture was heat treated in a H_2/Ar flow at 500 °C and 700 °C for 2 h, respectively. Finally, the Pt_3Co NPs supported on carbon were monodispersed in NaCl-matrix. Subsequently, the mixture was washed and centrifuged several times in deionized water to eliminate NaCl. The final products were dried in vacuum at 40 °C for 20 h and marked as Pt_3Co/C-500 and Pt_3Co/C-700, respectively.

Preparation of catalyst ink

To obtain catalyst ink (2 mg mL^{-1}), a specified amount of Pt_3Co/C was dispersed in a solution composed of distilled water, isopropanol, and Nafion (5%) ($v/v/v$ 3:1:0.05). Afterward, 10 μL of catalyst ink was loaded on an inverted glassy carbon (GC) disk electrode (5 mm diameter, spinning at 400 rpm) and dried at ambient condition [26].

Characterization of samples

Crystalline phases of samples were analyzed by an X-ray diffractometer (Rigaka Ultima IV) using Cu-Kα radiation over 5–95° (sweeping rate of 10°·min^{-1}). The hysteresis loop was investigated by a superconducting quantum interface device (SQUID). Morphologies and crystal structure were analyzed by transmission electron microscopy (JEOL JEM-2100HR). Elemental mappings and EDS line scanning profiles of Pt and Co elements were tested by transmission electron microscopy (FEI Tecnai G2 F20).

Electrochemical characterization

Electrochemical performance was tested by a three-electrode system with a rotation speed controller (PINE Research Instruments) combined with an electrochemical workstation (CHI 660D, CH Instruments, Inc.) in 0.1 M $HClO_4$ acid. Reference electrode was Ag/AgCl (3 M KCl), and counter electrode was platinum wire, respectively. Linear sweep voltammetry (sweep rate of 20 mV·s^{-1}) and potential cycles (sweep rate of 50 mV·s^{-1}) were record to characterize the activity and durability toward ORR over 0.05–1.1 V (vs. RHE), respectively.

Results and discussion

Typical synthesis of ordered Pt_3Co/C NPs is illustrated in Fig. 1. Firstly, a uniformly precursor solution containing a certain amount of cobaltous chloride, chloroplatinic acid, sodium chloride, PVP, and carbon black is prepared (Fig. 1a). Secondly, the precursor solution was sprayed onto a quartz plate (kept at 270 °C). (Fig. 1b). A uniformly mixed salt precursor was formed at the surface of the quartz plate for the solvent evaporated off instantly and each component precipitate simultaneously (Fig. 1c). Third, a post heat treatment is conducted to obtain Pt_3Co/C NPs (Fig. 1d). The bulk Pt-Co alloy phase diagram reflects that the ordered phase (primitive cubic) is more thermodynamic stable compared to disordered phase (fcc) below 750 °C [27, 28]. However, we often obtain a

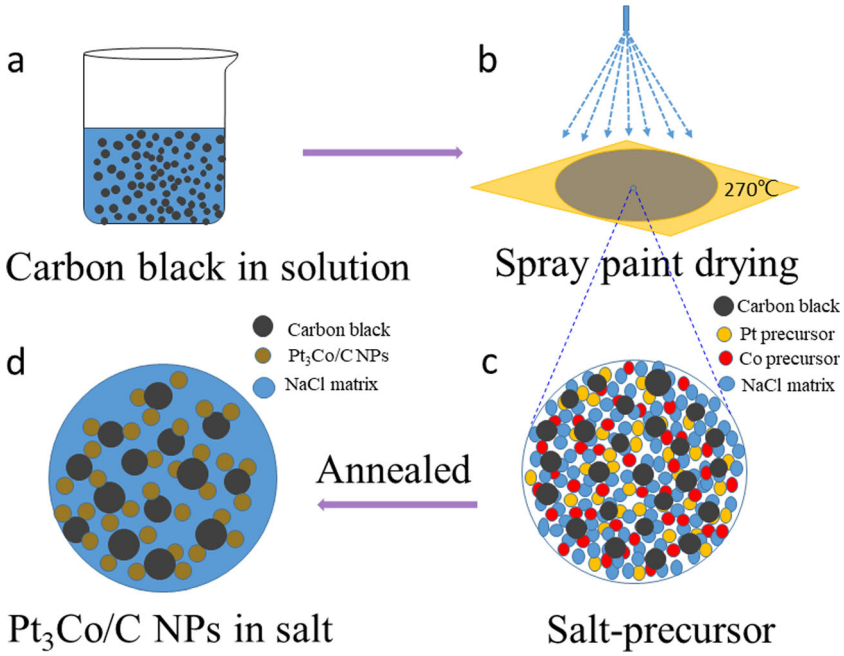

Fig. 1 Schematic illustration for the synthesis of chemically ordered Pt_3Co/C NPs

disordered structure prepared by a common method. To reach an ordered arrangement of atoms, high temperature heat treatment is usually needed [29].

Typical XRD patterns of as-synthesized Pt_3Co/C NPs annealed at different temperatures are given in Fig. 2a. The sample Pt_3Co/C-500 shows four obvious diffraction peaks at 40.5°, 47.1°, 68.8°, and 83.0°, indexed to (111), (200), (220), and (311) planes of fcc Pt_3Co, respectively. The XRD pattern of the sample Pt_3Co/C-700 presents a good crystallized structure of $L1_2$-Pt_3Co, as evidenced by two additional diffraction peaks appearing at 23.1° and 32.8° indexed to (100) and (110) planes compared with the fcc-Pt_3Co, respectively. Furthermore, no other diffraction peaks are detected from the platinum, cobalt, or any other impurities, which indicates the well alloying of platinum and cobalt in designed proportion. In addition, the magnetic properties of as-prepared samples were measured by SQUID. As seen in the M-H curves (Fig. 2b), the saturation magnetization (M_S) increases from 12 emu/g to 21.3 emu/g with higher annealing temperature. It could be ascribed to growth of the particle size caused by higher annealing temperature [30]. As found in the hysteresis loop (Fig.2b), the coercivity measured at 300K is close to zero, much less than 500 Oe at 2 K. This is attributed to thermal energy playing a dominant role in competition with magnetocrystalline anisotropy energy, resulting in a superparamagnetic behavior [31].

To further confirm the alloying of Pt and Co metal, the HAADF-STEM images, elemental mappings, and EDS line scanning profiles of Pt_3Co/C-700 NPs have been provided in Fig. 3. It is obvious that Pt and Co elements are well-distributed

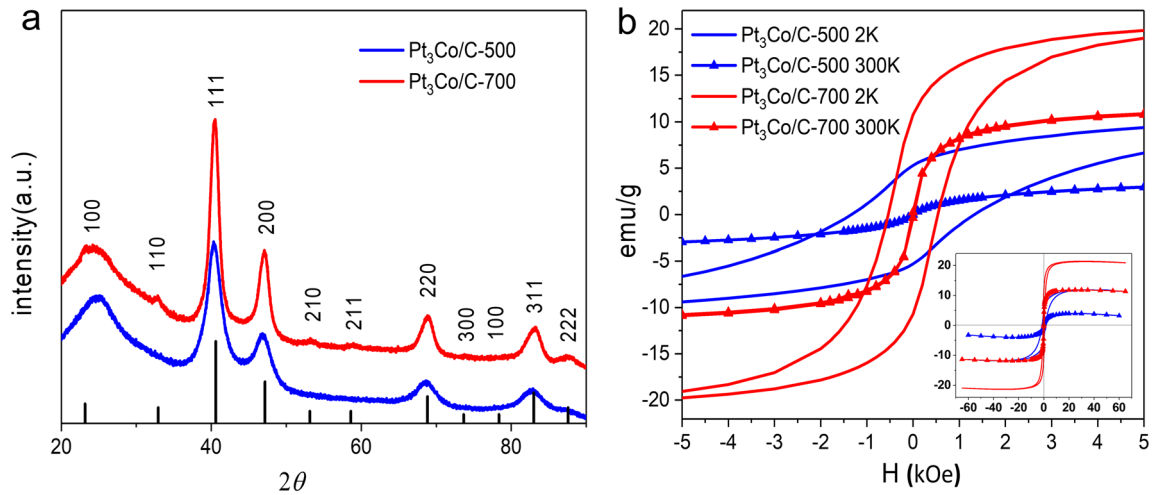

Fig. 2 **a** XRD patterns of Pt_3Co/C-500 and Pt_3Co/C-700. **b** Magnetic hysteresis loops of Pt_3Co/C-500 and Pt_3Co/C-700 measured at 2 K and 300 K

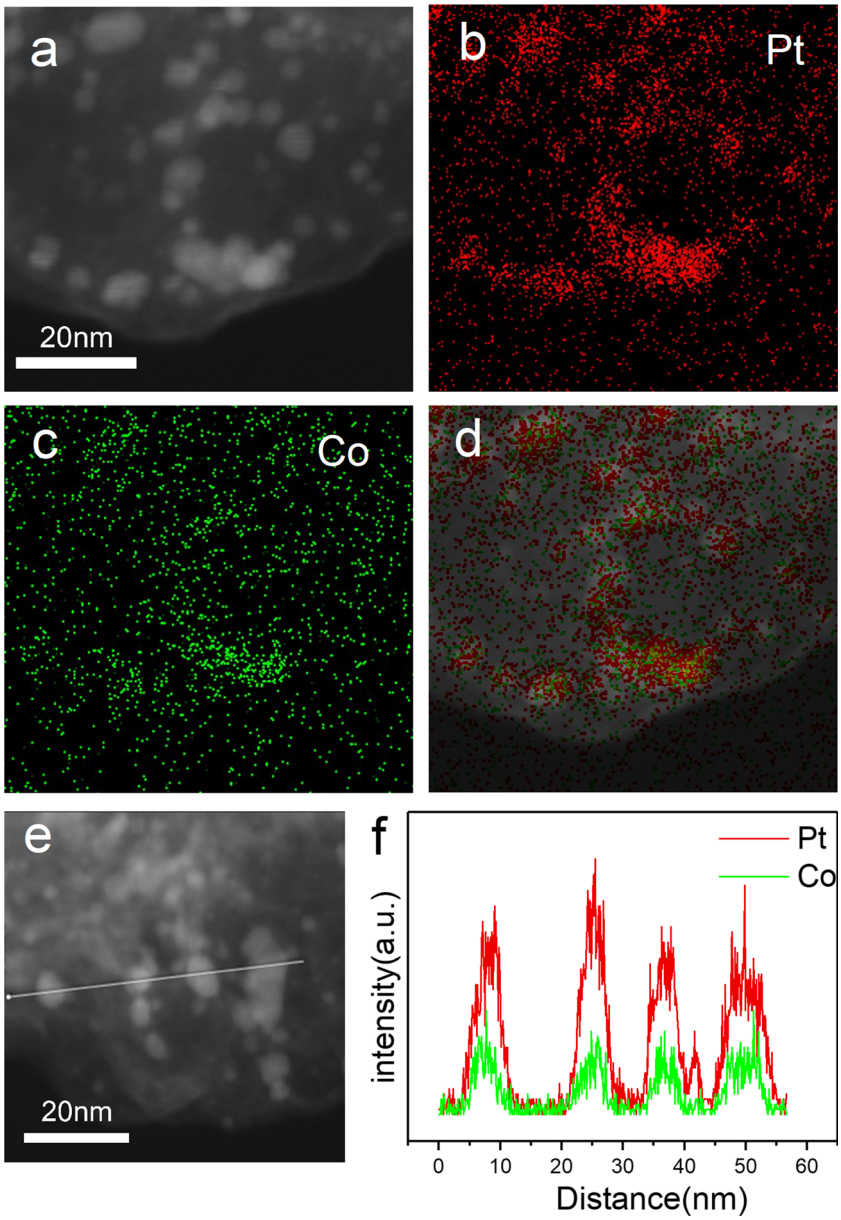

Fig. 3 **a** HAADF-STEM images of Pt_3Co/C-700 NPs. **b–d** Elemental mappings for Pt and Co elements. **e, f** EDS line scanning profiles of Pt and Co elements

in the nanoparticles, indicating the well alloying of Pt and Co metal in Pt_3Co/C-700 NPs obtained by our synthetic strategy.

We further investigated the structure and morphology of as-synthesized products by using TEM. Confirmed by the low-resolution TEM images (Fig. 4a, c), the Pt_3Co particles are monodisperse and homogeneous on carbon black. Clearly, the HRTEM image (Fig. 4b, d) presents the lattice spacing of 2.2 Å, in agreement with a cubic crystallographic Pt_3Co structure. As shown, the Pt_3Co/C-700 NPs present polygon morphology compared to spherical morphology of Pt_3Co/C-500 NPs. The predominantly exposed facets are (111) plane in the Pt_3Co/C-700 NPs [32]. Fig. 4e shows the corresponding size distribution histograms obtained by analyzing TEM images using the particle size analysis software package. The synthesized Pt_3Co/C-500 NPs show a narrow size distribution with an average size of 4.4 nm, and the average size of Pt_3Co/C-700 NPs is about 5.1 nm. Consequently, the particle size increase slightly annealed at 700°C, which is smaller than that of Wang et al. (7.2±1 nm) prepared by an impregnation method [17]. In order to investigate the effect of NaCl-matrix in the experiment, the synthesis experiment without adding NaCl-matrix was taken out. Low- and high-magnification TEM images of S500 and S700 NPs are shown in Figs. S2 and S3 (Supporting Information). It can be observed that the Pt_3Co NPs prepared without adding NaCl-matrix show a serious agglomeration. Consequently, NaCl-matrix also plays a vital role in hindering agglomeration of Pt_3Co nanoparticles during annealing. Thus, it can be seen that carbon black and sodium chloride play a vital role in hindering agglomeration of Pt_3Co nanoparticles during high temperature annealing. And it is

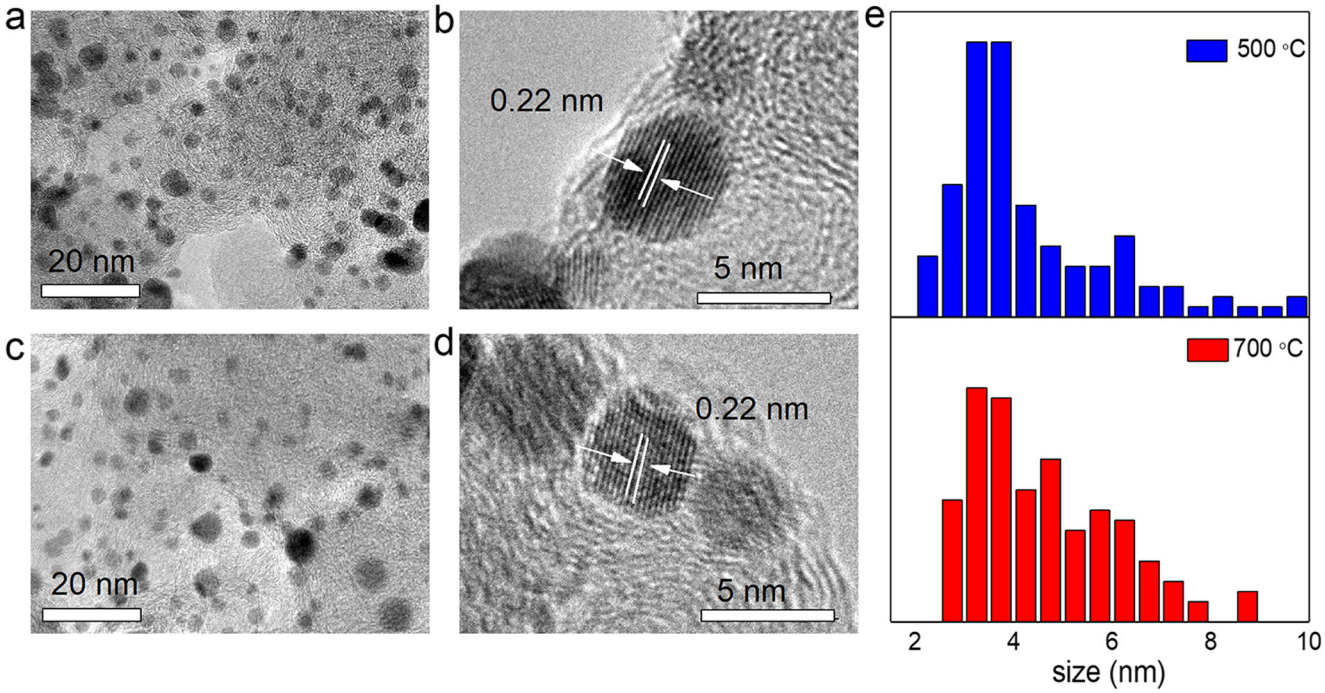

Fig. 4 **a, b** Low- and high-resolution TEM images of Pt_3Co/C-500 NPs. **c, d** Low- and high-resolution TEM images of Pt_3Co/C-700 NPs. **e** The size distribution histograms of Pt_3Co/C-500 and Pt_3Co/C-700

worth emphasizing that decreasing the size of Pt-based alloy nanoparticles is a critical way to raise the utilization of Pt.

The prepared Pt_3Co/C-500 and Pt_3Co/C-700 NPs were served as electrocatalysts for the ORR to investigate the difference in the electrocatalytic performance. To remove contamination on the surface of NPs, 50 CV cycles (in O_2-saturated 0.1 M $HClO_4$ acid, 50 $mV{\cdot}s^{-1}$) are conducted before ORR measurements. Clearly, the onset potential and half-wave potential ($E_{1/2}$) of Pt_3Co/C-700 catalysts are both higher than Pt_3Co/C-500 and Pt/C catalysts observed from the polarization curves in Fig. 5a. The $E_{1/2}$ of Pt_3Co/C-500 and Pt_3Co/C-700 were 0.900 V and 0.912 V, exhibiting 24 mV and 36 mV higher than Pt/C (0.876 V). These results indicate that the ordered Pt_3Co/C electrode owns a significantly improved catalytic activity compared to the chemically disordered Pt_3Co/C and Pt/C.

To more intuitively illustrate the difference of ORR activities between the prepared electrocatalysts and commercial Pt/C, the mass activities displyed in Fig. 5b were calculated at 0.85 and 0.90 V by the Koutecky–Levich (K–L) equation:

$$I^{-1} = I_d{}^{-1} + I_k{}^{-1} \quad (1)$$

where I, I_d, and I_k is the measured, diffusion limited, and kinetic current, respectively. Meanwhile, I_d could be expressed by the Levich equation:

$$I_d = 0.62nFAD^{2/3}v^{-1/6}w^{1/2}C_{O_2} \quad (2)$$

where n is the electron transfer number per molecule of oxygen; F is the Faraday constant (96485 C mol^{-1}); C_o is the bulk concentration of oxygen in 0.1 M $HClO_4$ solution (1.26×10^{-6} mol cm^{-3}); A is the area of the glassy carbon electrode (0:1964 cm^2); D is the diffusion coefficient of oxygen (1.93×10^{-5} cm^2 s^{-1}); v is the kinetic viscosity of electrolyte (1.01×10^{-2} cm^2 s^{-1}); and ω is the angular velocity of rotation [17].

As seen in Fig. 5b, the Pt_3Co/C-700 exhibits the best mass activity (0.62 mA $\mu g_{Pt}{}^{-1}$ at 0.85 V, 0.21 mA $\mu g_{Pt}{}^{-1}$ at 0.90 V), which are 2.4-fold and 2.51-fold of commercial Pt/C (0.261 mA $\mu g_{Pt}{}^{-1}$ at 0.85 V, 0.084 mA $\mu g_{Pt}{}^{-1}$ at 0.90V). Meanwhile, the Pt_3Co/C-500 shows 1.76 and 1.81 times enhancement than commercial Pt/C. These results reveal that chemical-ordered structure enhanced the catalytic activity markedly.

Figure 5c shows the LSV curves of Pt_3Co/C-700 catalyst measured at different rotating speeds. The K–L plot of I^{-1} versus $w^{-1/2}$ presents a linear relationship. According to the slope of K–L curves, the reaction is a 4-electron transfer process, which confirms that O_2 is completely reduced to H_2O without intermediate of hydrogen peroxide (H_2O_2). In order to further comprehend the effects of alloying with transition metal cobalt and crystal structure in the catalysts, the Tafel plots are displayed in Fig. 5d over 0.85–1.00 V. Clearly, the kinetic current density increased in the following sequence: Pt/C < Pt_3Co/C-500 < Pt_3Co/C-700 at an arbitrary potential; further signifying chemically ordered Pt_3Co/C-700 catalysts exhibit an excellent catalytic performance superior to commercial Pt/C and Pt_3Co/C-500.

To explore the durability of as-synthesized NPs, the catalysts were examined through an accelerated durability test (ADT) conducted under O_2-saturated condition over 0.05–

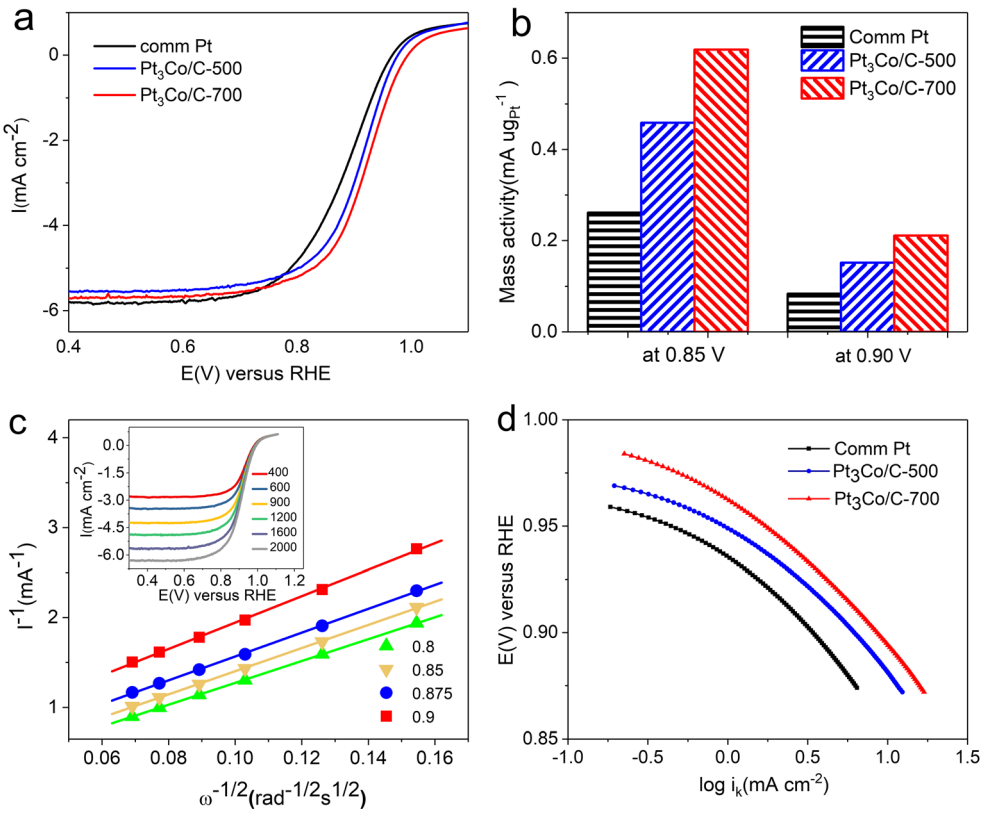

Fig. 5 **a** Linear sweep voltammetry (LSV) curves for comm Pt/C, Pt_3Co/C-500, and Pt_3Co/C-700 measured at ambient temperature in an O_2-saturated 0.1M $HClO_4$ acid (scanning rate of 20 mV·s^{-1}, rotation rate of 1600 rpm). **b** Comparative mass activities at 0.85 V and 0.9 V. **c** The K-L plots of Pt_3Co/C-700 acquired from ORR polarization curves at different potentials. Inset: ORR polarization curves at different rotation rates. **d** Tafel plots of commercial Pt/C, Pt_3Co/C-500, and Pt_3Co/C-700

1.1 V for 5 000 and 10000 cycles. Fig. 6a and b exhibit the cyclic voltammetry (CV) profiles tested in N_2-purged electrolyte. Clearly, the Pt_3Co/C-700 NPs do not show any signal activity degeneration. The electrochemical activity area ECSA (listed in Table 1) was calculated by integrating the function (Eq. 3) on the hydrogen desorption region of the cyclic voltammetry curves.

$$A = \frac{Q_H}{[\mathrm{Pt}]\cdot 0.2} \tag{3}$$

where A is electrochemical surface area (ECSA), [Pt] is the mass of platinum loaded on unit area of glassy carbon electrode, and Q_H is the charge of hydrogen desorption.

As listed in Table 1, with the increase of potential cycles (0, 5000, and 10000), the electrochemical active area (ECSA) of Pt_3Co/C-500 changed from 76.3 to 59.7 and finally stabilizes at 59.8 m^2 g^{-1} (Pt). However, the Pt_3Co/C-700 sample changed from 61.6 to 62.9 and finally stabilized at 63.8 m^2 g^{-1} (Pt). It can be seen that Pt_3Co/C-500 suffered from almost 22% loss. However, Pt_3Co/C-700 increased by 3.6% after 10000 potential cycles. To better understand the enhancement of durability, the ORR activities before and after 10000 potential sweeps are exhibited in Fig. 6d. Apparently, the Pt_3Co/C-700 catalyst do not show distinct activity attenuation and reflect $E_{1/2}$ negative shift as low as 15 mV after 10000 CV cycles. However, the Pt_3Co/C-500 catalyst shows approximately 40 mV-negative shift. To more intuitively illustrate the activity evolutions of the catalyst, the mass activities after various potential-scanning cycles were calculated and are shown in Fig. 6e and f. To be exact, the comm Pt, Pt_3Co/C-500, and Pt_3Co/C-700 suffered from 51.3%, 67.6%, and 36.3% loss of initial mass activities after 10000 potential cycles. Apparently, the Pt_3Co/C-700 presents the best mass activity and durability toward ORR. The Pt_3Co/C-700 NPs possessing superior ORR performance may ascribe to the ideal catalytic facets exposed at the surface of Pt_3Co/C-700 NPs (Fig. 4d). Meanwhile, the cobalt ion etching was restrained for their ordered structure [33]. Furthermore, synergy arising from the electronic spin-orbit coupling between Co and Pt makes the $L1_2$-Pt_3Co chemically much more active and stable [34]. Besides, carbon black and sodium chloride play as

Table 1 ECSA of synthesized catalysts suffered from different potential cycles

Sample	Pt_3Co/C-500 ECSA (m^2 g^{-1}) (Pt)	Pt_3Co/C-700 ECSA (m^2 g^{-1}) (Pt)
Initial	76.3	61.6
5000 cycles	59.7	62.9
10000 cycles	59.8	63.8

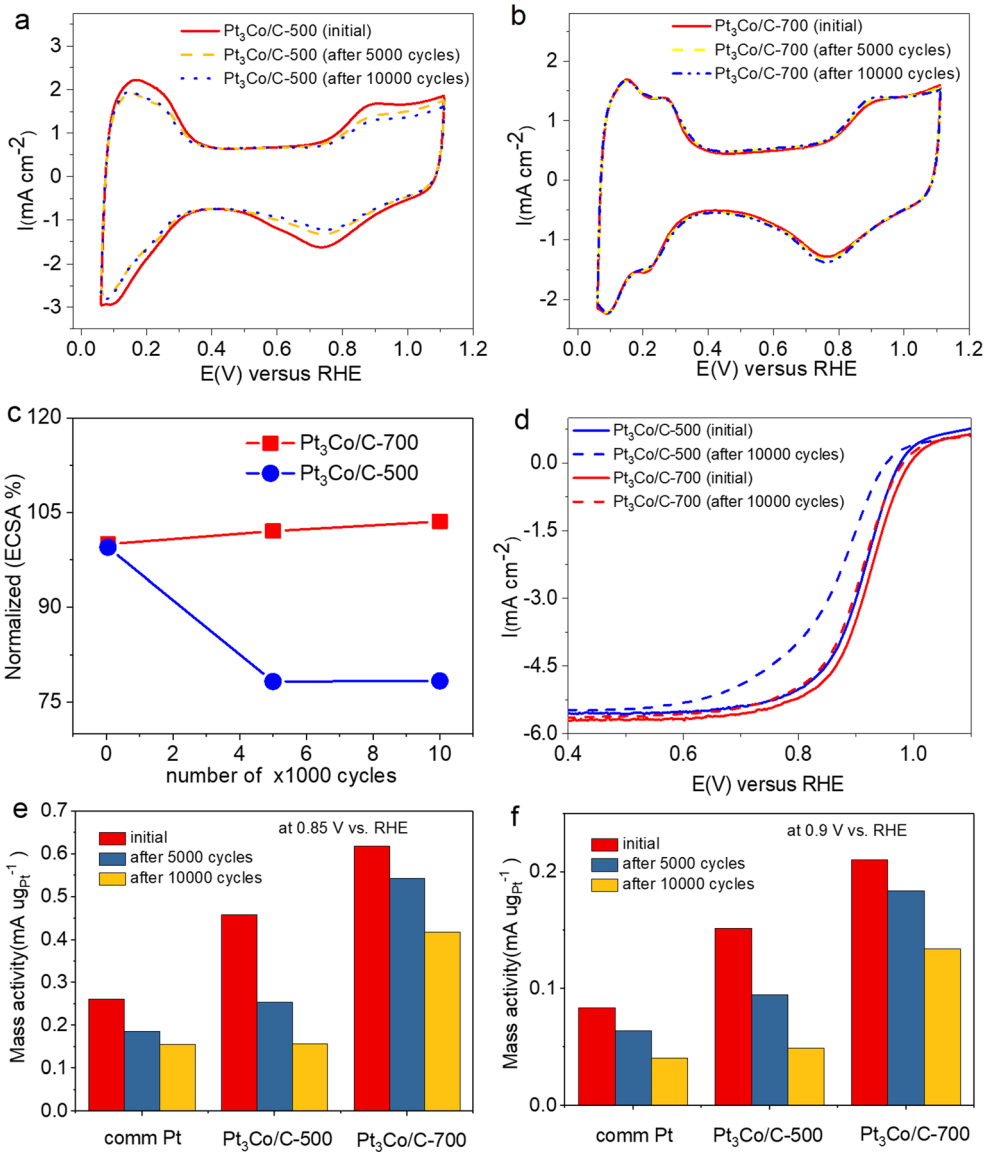

Fig. 6 CV profiles of **a** Pt_3Co/C-500 and **b** Pt_3Co/C-700 measured in N_2-purged 0.1 M $HClO_4$ solution after different potential cycles in O_2-saturated 0.1 M $HClO_4$ acid with a scanning rate of 50 $mV{\cdot}s^{-1}$. **c** Electrochemical surface area (ECSA) of Pt_3Co/C-500 and Pt_3Co/C-700 catalysts changes with the CV cycles. **d** Electrocatalytic stability tests of Pt_3Co/C-500 and Pt_3Co/C-700 before and after 10000 potential cycles. **e, f** Comparison of mass activities for different catalysts before and after ADTs at 0.85 V and 0.9 V, respectively

an alloying reactor impeding the sintering and growth of Pt_3Co alloy NPs during high temperature annealing, which guarantee a sufficient active area for catalytic reaction.

Conclusion

In summary, this work presents a solid phase method to realize the ordered Pt_3Co nanoparticles monodispersed on carbon black. The obtained chemically ordered Pt_3Co NPs show small average diameter and narrow size distribution. And it exhibits enhanced ORR catalytic activity and outstanding stability in protecting Co ions from etching in acid relative to disordered phase. Compared with the traditional impregnation method, this method is fast and environmental friendly. Meanwhile, the proportion of components can be precisely controlled, no need of considering the different adsorption capacity of ions on the carrier. Such simple synthetic strategy can also be extended to prepare other durably active ordered intermetallic electrocatalysts for fuel cell applications.

Supplementary Information The online version contains supplementary material available at https://doi.org/10.1007/s11581-021-04017-w.

Acknowledgements This work was supported by the National Natural Science Foundation of China (Grant No. 11604147) and the Foundation of National Laboratory of Solid State Microstructures, Nanjing University (M32048).

Declarations

Conflict of interest The authors declare no conflicts of interest.

References

1. Li J, Yin HM, Li XB, Okunishi E, Shen YL, He J, Tang ZK, Wang WX, Yücelen E, Li C, Gong Y, Gu L, Miao S, Liu LM, Luo J, Ding Y (2017) Surface evolution of a Pt–Pd–Au electrocatalyst for stable oxygen reduction. Nat Energy 2(8):17111
2. Kulkarni A, Siahrostami S, Patel A, Nørskov JK (2018) Understanding catalytic activity trends in the oxygen reduction reaction. Chem Rev 118(5):2302–2312
3. Liu ML, Zhao ZP, Duan XF, Huang Y (2019) Nanoscale structure design for high-performance Pt-Based ORR catalysts. Adv Mater 31(6):1–8
4. Debe MK (2012) Electrocatalyst approaches and challenges for automotive fuel cells. Nature 486(7401):43–51
5. Li MF, Zhao ZP, Cheng T, Fortunelli A, Chen CY, Yu R, Zhang QH, Gu L, Merinov BV, Lin ZY, Zhu E, Yu T, Jia QY, Guo JH, Zhang L, Goddard WA, Huang Y, Duan XF (2016) Ultrafine jagged platinum nanowires enable ultrahigh mass activity for the oxygen reduction reaction. Science 354(6318):1414–1419
6. Wu BH, Wu CQ, Zhu JJ, Xue L, Chu J, Wang XQ, Xiong SX (2020) Facile synthesis of carboxylated-graphene nanosheets supported PtRu catalysts and their electrocatalytic oxidation of methanol. Ionics 26:4599–4608
7. Ren WN, Zang WJ, Zhang HF, Bian JL, Chen ZF, Guan C, Cheng CW (2019) PtCo bimetallic nanoparticles encapsulated in N-Doped carbon nanorod arrays for efficient electrocatalysis. Carbon 142:206–216
8. Wang C, Vliet DVD, More KL, Zaluzec NJ, Peng S, Sun SH, Daimon H, Wang GF, Greeley J, Pearson J, Paulikas PA, Karapetrov G, Strmcnik D, Markovic NM, Vojis A (2011) Multimetallic Au/$FePt_3$ nanoparticles as highly durable electrocatalyst. Nano Lett 11(3):919–926
9. Xin HL, Alayoglu S, Tao R, Genc A, Wang CM, Kovarik L, Stach EA, Wang LW, Salmeron M, Somorjai GA, Zheng HM (2014) Revealing the atomic restructuring of Pt-Co nanoparticles. Nano Lett 14(6):3203–3207
10. Zhai XH, Wang P, Wang K, Jun L, Pang XL, Wang X, Zhao L (2020) Facile synthesis of PtCo nanowires with enhanced electrocatalytic performance for ethanol oxidation reaction. Ionics 26:3091–3097
11. Stamenkovic VR, Mun BS, Mayrhofer KJJ, Ross PN, Markovic NM (2006) Effect of surface composition on electronic structure, stability, and electrocatalytic properties of Pt-transition metal alloys: Pt-skin versus Pt-skeleton surfaces. J Am Chem Soc 128(27):8813–8819
12. Liang J, Li N, Zhao Z, Ma L, Wang X, Li S, Liu X, Wang T, Du Y, Lu G, Han J (2019) Tungsten-doped L_{10}-PtCo ultrasmall nanoparticles as a high-performance fuel cell cathode. Angew Chem 131(43):15617–15623
13. Zhang L, Roling LT, Wang X, Vara M, Chi MF, Liu JY, Choi S, Park JH, Herron JA, Xie ZX, Mavrikakis M, Xia YN (2015) Platinum-based nanocages with subnanometer-thick walls and well-defined, controllable facets. Science 349(6246):412–416
14. Greeley J, Stephens IEL, Bondarenko AS, Johansson TP, Hansen HA, Jaramillo TF, Rossmeisl J, Chorkendorff I, Nørskov JK (2009) Alloys of platinum and early transition metals as oxygen reduction electrocatalysts. Nat Chem 1(7):552–556
15. Ling LL, Liu WJ, Chen SQ, Hu X, Jiang H (2018) MOF templated nitrogen doped carbon stabilized Pt–Co bimetallic nanoparticles: low Pt content and robust activity toward electrocatalytic oxygen reduction reaction. ACS Appl Nano Mater 1(7):3331–3338
16. Kimmel YC, Xu XG, Yu WT, Yang XD, Chen JG (2014) Trends in electrochemical stability of transition metal carbides and their potential use as supports for low-cost electrocatalysts. ACS Catal 4(5):1558–1562
17. Wang DL, Xin HL, Hovden R, Wang HS, Yu YC, Muller DA, DiSalvo FJ, Abruna HD (2013) Structurally ordered intermetallic platinum-cobalt core-shell nanoparticles with enhanced activity and stability as oxygen reduction electrocatalysts. Nat Mater 12(1):81–87
18. Hunt ST, Milina M, Alba-Rubio AC, Hendon CH, Dumesic JA, Román-Leshkov Y (2016) Self-assembly of noble metal monolayers on transition metal carbide nanoparticle catalysts. Science 352(6288):974–978
19. Li Q, Wu LH, Wu G, Su D, Lv HF, Zhang S, Zhu WL, Casimir A, Zhu HY, Mendoza-Garcia A, Sun SH (2015) New approach to fully ordered fct-FePt nanoparticles for much enhanced electrocatalysis in acid. Nano Lett 15(4):2468–2473
20. Rong CB, Li DR, Nandwana V, Poudyal N, Ding Y, Wang ZL, Zeng H, Liu JP (2006) Size-dependent chemical and magnetic ordering in $L1_0$-FePt nanoparticles. Adv Mater 18(22):2984–2988
21. Lokanathan M, Patil IM, Mukherjee P, Swami A, Kakade B (2020) Molten-salt synthesis of Pt_3Co binary alloy nanoplates as excellent and durable electrocatalysts toward oxygen electroreduction. ACS Sustain Chem Eng 8(2):986–993
22. Chen YZ, Xu Q, Yu SH, Jiang HL (2014) Tiny Pd@Co core-shell nanoparticles confined inside a metal-organic framework for highly efficient catalysis. Small 11(1):71–76
23. Chong S, Zhang GM, Zhang N, Liu YC, Zhu J, Huang T, Fang SY (2016) Preparation of FeCeOx by ultrasonic impregnation method for heterogeneous fenton degradation of diclofenac. Ultrason Sonochem 32:231–240
24. Behzadnia A, Montazer M, Rad MM (2015) In-situ sonosynthesis of nano N-doped ZnO on wool producing fabric with photo and bio activities, cell viability and enhanced mechanical properties. J Photoch Photobio B 149:103–115
25. Cheng ZZ, Geng XP, Chen LY, Zhang C, Huang HH, Tang SL, Du YW (2018) In situ synthesis of chemically ordered primitive cubic Pt_3Co nanoparticles by a spray paint drying method for hydrogen evolution reaction. J Mater Sci 53(17):12399–12406
26. Garsany Y, Ge JJ, St-Pierre J, Rocheleau R, Swider-Lyons KE (2014) Analytical procedure for accurate comparison of rotating disk electrode results for the oxygen reduction activity of Pt/C. J Electrochem Soc 161(5):628–640
27. Wen YH, Zhang LH, Wang JB, Huang R (2019) Atomic-scale insights into thermal stability of Pt_3Co nanoparticles: a comparison between disordered alloy and ordered intermetallics. J Alloys Compd 776:629–635
28. Hansen M, Anderko K (1958) Constitution of binary alloys, 2nd edn. McGraw-Hill, New York
29. Berg H, Cohen JB (1972) Long-range order and ordering kinetics in $CoPt_3$. Metall Trans 3(7):1797–1805
30. Murray CB, Sun SH, Doyle H, Betley T (2001) Monodisperse 3d transition-metal (Co, Ni, Fe) nanoparticles and their assembly into nanoparticle superlattices. MRS Bull 26(12):985–991
31. Sánchez-Barriga J, Lucas M, Radu F, Martin E, Multigner M, Marin P, Hernando A, Rivero G (2009) Interplay between the magnetic anisotropy contributions of cobalt nanowires. Phys Rev B 80(18):1–8
32. Wakisaka M, Mitsui S, Hirose Y, Kawashima K, Uchida H, Watanabe M (2006) Electronic structures of Pt-Co and Pt-Ru alloys for CO-tolerant anode catalysts in polymer electrolyte fuel cells studied by EC-XPS. J Phys Chem B 110(46):23489–23496
33. Kim J, Lee YM, Sun SH (2010) Structurally ordered FePt nanoparticles and their enhanced catalysis for oxygen reduction reaction. J Am Chem Soc 132(14):4996–4997
34. Šipr O, Minár J, Mankovsky S, Ebert H (2008) Influence of composition, many-body effects, spin-orbit coupling, and disorder on magnetism of Co-Pt solid-state systems. Phys Rev B 78(14):1–12